Applied Energy 304 (2021) 117767

Contents lists available at ScienceDirect

Applied Energy

journal homepage: www.elsevier.com/locate/apenergy

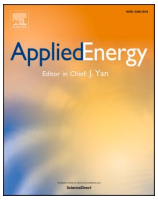

CO_2 capture using ionic liquid-based hybrid solvents from experiment to process evaluation

Chunyan Ma [a,*], Nan Wang [a], Nannan Ye [b], Xiaoyan Ji [a,*]

[a] Energy Engineering, Department of Engineering Science and Mathematics, Luleå University of Technology, Luleå 97187, Sweden
[b] Key Laboratory of Material and Chemical Engineering, Nanjing Tech University, Nanjing 210009, China

HIGHLIGHTS

- [Bmim][OAc] based hybrid solvents were investigated for CO_2 capture.
- Cosolvent effect on CO_2 solubility has been studied, and the preferable one is selected.
- CO_2 solubilities at different temperatures and cosolvent contents were tested and modeled.
- The effect of N_2 in the gas stream on the CO_2 absorption capacity is negligible.
- The hybrid solvent decreases 52% utility cost and 11% capture cost than the MEA process.

ABSTRACT

The CO_2 absorption capacity in three hybrid solvents based on butyl-3-methylimidazolium acetate ([Bmim][OAc]) and three different cosolvents (Dimethyl ethers of polyethylene glycol (DEPG250), propylene carbonate, and water) was investigated and compared, and [Bmim][OAc]-DEPG250 shows the highest CO_2 absorption capacity. The effects of the mass ratio of [Bmim][OAc]-DEPG250 and temperature on their CO_2 absorption capacity, density, and viscosity were further investigated. In addition, the absorption capacities of N_2 and CO_2 in [Bmim][OAc]-DEPG250 with the simulated flue gas as a feed gas were studied and compared with that using the pure gas as a feed gas. Thermodynamic models were used to represent the experimental data, and then process simulation and evaluation were carried out. The results show that the addition of DEPG250 dramatically decreases the viscosity, while the absorption capacity of hybrid solvents is still comparable with pure [Bmim][OAc]. The type of gas stream, that is, pure gas or gas mixture, has a negligible effect on the N_2 and CO_2 absorption capacity. The simulation results show that [Bmim][OAc]-DEPG250 only utilizes less than 50% of the heating duty of aqueous amine solution because of the low-pressure desorption and preheating with waste heat in this hybrid solvent-based process. The CO_2 capture cost of using this [Bmim][OAc]-DEPG250 reduces by 11% compared with that of using aqueous amine solution due to the significant decrease (by 52%) in utility cost.

1. Introduction

Carbon dioxide (CO_2), which accounts for 76% of total anthropogenic greenhouse gas (GHG) emissions, is the primary concern of reducing the climate change effect. Currently, solvent-based absorption technologies are the most commercial-ready technology for CO_2 capture. Amine-based absorbents, such as monoethanolamine (MEA), diethanolamine (DEA), and N-methyldiethanolamine (MDEA), are the widely studied chemical absorbents in CO_2 capture from flue gas as their pronounced high CO_2 absorption capacity [1]. However, the high energy penalty of solvent regeneration, high solvent volatility, solvent degradation, and equipment corrosion limit their applications. Therefore, new solvent development to overcome all these drawbacks is vital.

Ionic liquids (ILs) have attracted a lot of attention as a feasible alternative to current conventional solvents because of their superior properties such as negligible vapor pressure, high thermal stability, good CO_2 uptake ability, tuneable property, and low energy demand for regeneration [2]. Research work has shown that the anions of ILs have a strong influence on CO_2 solubility, and the one with acetate $[OAc]^-$ as the anion shows the highest CO_2 absorption capacity among the investigated conventional imidazolium-based ILs [3]. Furthermore, 1-butyl-3-methylimidazolium acetate ([Bmim][OAc]) has been widely studied for CO_2 capture from experimental measurement to process simulation and proposed as one of the potential IL candidates for CO_2 capture in the Technical Reports from DOE (Department of Energy, USA) [4]. The work from Yokozeki et al. [5] shows that similar to other ILs, [Bmim][OAc] is with the characteristics of both physical and chemical absorption. Later, Shiflett et al. [6] studied CO_2 solubility at various temperatures and

* Corresponding authors.
E-mail addresses: chunyan.ma@ltu.se (C. Ma), xiaoyan.ji@ltu.se (X. Ji).

https://doi.org/10.1016/j.apenergy.2021.117767
Received 21 April 2021; Received in revised form 8 July 2021; Accepted 26 August 2021
Available online 10 September 2021

pressures. Subsequently, Shiflett et al. [7] simulated CO_2 capture from flue gas using pure Bmim][OAc] and claimed a 16% reduction in energy usage and 11 % reduction in investment cost compared with aqueous amine scrubbing. Considering that the work by Shiflett et al. [7] was for the flue gas at a low flow rate and the process was simplified, based on the parameters from Shiflett et al. [7], Nguyen et al.[8] developed a complete [Bmim][OAc]-based CO_2 capture process including dehydration, CO_2 capture, and compression steps. The results show that compared to the MEA process, [Bmim][OAc]-based processes are only quite economical when the flow rate of flue gas and CO_2 content are high. The simulation results of CO_2 capture for the pure [Bmim][OAc] show the potential of energy-saving, and it is more environmentally friendly because of less evaporation compared to conventional amine-based solvents. However, the viscosity of [Bmim][OAc] is very high, which is around 383 mPa s [9] for [Bmim][OAc] with 2.9 wt% water at 298.15 K, that is, 430 times of water. This high viscosity makes it hard to use pure [Bmim][OAc] in a solvent-based CO_2 absorption process.

Adding cosolvents has been proposed as a solution to overcome the limitation of the high viscosity of IL [10]. Water is a green cosolvent with low viscosity, and in general, the addition of water leads to a significant reduction in viscosity and decreases CO_2 absorption capacity to some extent [11-13]. Even though the CO_2 absorption capacity of aqueous IL is lower than pure IL, the use of aqueous IL still can reduce the energy usage and equipment size in CO_2 separation from biogas compared with other conventional physical solvents [14]. Besides water, organic solvents such as polyethylene glycol (PEG), dimethyl ethers of polyethylene glycol (DEPG) have also been studied as cosolvents to decrease the viscosity. Li et al. [15] studied the influence of additional PEG in (2-hydroxyethyl)-trimethyl-ammonium (S)-2-pyrrolidine carboxylic acid salt ([Choline][Pro]), showing that PEG enhances CO_2 absorption- and desorption-rate significantly. The results of Lepre et al.[16] show that adding DEPG with a molecular weight less than 1000 as a cosolvent can greatly decrease the viscosity when using butyl-trimethylammonium bis(trifluoromethyl sulfonyl) imide IL ($[N_{4111}][Tf_2N]$), meanwhile, increase CO_2 solubility. As mentioned by Maginn [4], the CO_2 removal processes with the features of the physical absorption and also the properties of chemical absorption are desirable to overcome the limitation of conventional physical and chemical processes. Therefore, adding cosolvent to form an IL-formulated hybrid solvent with the features of chemical and physical absorptions and studying the cosolvent effect are of great interest. The comparison of the performance of CO_2 capture with these hybrid solvents and the conventional amine solutions in terms of energy and cost is quite important.

In this work, the CO_2 absorption capacity of [Bmim][OAC] with water, DEPG250, and propylene carbonate (PC) formulated hybrid solvents were studied and compared to identify the preferable cosolvent. After that, the effects of mass ratio and temperature on CO_2 absorption capacity, density, and viscosity of the [Bmim][OAC] with the identified cosolvent were studied at pressures from 0 to 1.9 MPa. Furthermore, the absorption capacity of pure N_2 was measured, and the effect of N_2 on the CO_2 absorption capacity was tested by measuring the gas absorption capacity with the flue gas (with 75 % N_2 and 25% CO_2) as an inlet gas. All these newly measured experimental data, together with the one from the literature, were used to model the gas absorption in these [Bmim][OAC]-formulated hybrid solvents based on the Non-random two-liquid model (NRTL) and Redlich-Kwong equation of state (RK). The physical properties, including density, viscosity, heat capacity and surface tension, were modeled with the equations in Aspen Plus. After that, process simulation and evaluation were carried out to study the performance (energy and cost) of the hybrid solvent, and the results were compared with that of the aqueous MEA based process.

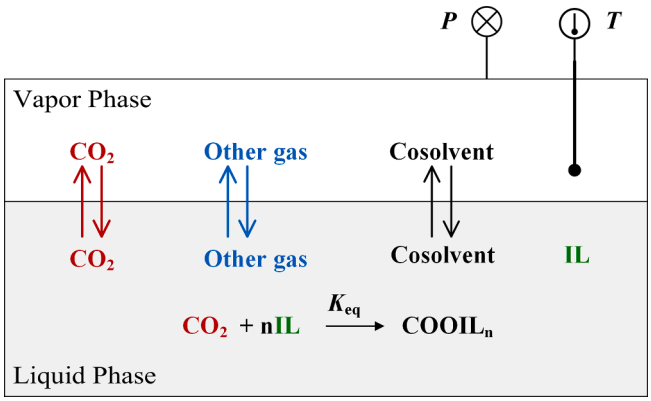

Fig. 1. Schematic of gas–liquid equilibria with chemical interaction. In this work, n is equal to 2, IL represents [Bmim][OAc], and $COOIL_n$ represents the reaction product [Bmim-2-COO].

2. Experiments and methods

2.1. Experiments

2.1.1. Materials

The IL of butyl-3-methylimidazolium acetate ([Bmim][OAc]) was purchased from the Lanzhou Institute of Chemical Physics (LICP) of the Chinese Academy of Sciences (CAS). The IL was dried in a vacuum oven for 24 h before use to avoid the trace of moisture. Dimethyl ethers of polyethylene glycol (DEPG250, average $M_n \sim 250$) and propylene carbonate (PC, purity 99.5%) were purchased from Sigma-Aldrich Ltd. The CO_2 (mole fraction $\geq$ 99.9%), N_2 (mole fraction $\geq$ 99.5%) and gas mixtures (simulated flue gas with 25 vol% CO_2 /75 vol% N_2) were purchased from AGA AB (Linde group). High-quality deionized water (conductivity, less than0.055 $\mu S \cdot cm^{-1}$) was used in this work.

2.1.2. Density ρ and viscosity η measurement

The density and viscosity of the binary solvents were measured at different temperatures. The densities were measured by the Anton Paar DMA 5000 density meter. The density meter was calibrated with air and pure water before measuring the samples. The measurements of viscosity were carried out using the Anton Paar Lovis 2000 ME viscosity meter. The viscosity meter was also calibrated before measurement with the standard liquid (N7.5, N26, and N100 viscosity oil). The temperature uncertainty of the density meter and the viscosity meter are 0.01 K and 0.02 K, respectively. The detailed information on the measurement can be found in our previous work [10]. All the measurements of density and viscosity were repeated three times, and the average value was reported. The average relative deviations (*ARD*) of measured density and viscosity are 0.0001% and 3.33%, respectively.

2.1.3. Gas absorption measurements

The gas absorption capacity was measured based on the method reported in our previous work [17,18]. Considering the negligible vapor pressure of [Bmim][OAC], it was assumed that [Bmim][OAc] only existed in the liquid phase. The overall uncertainty for the measured gas absorption capacity was within $\pm$1.5%.

2.2. Theory of thermodynamic modeling

In this work, two pure gases (CO_2 and N_2) and one gas mixture (75 vol% N_2, 25 vol% CO_2) were involved. It has been proved that both physical and chemical interactions exist between CO_2 and [Bmim][OAc], while there are only physical interactions between CO_2 and the cosolvents investigated in this work [5]. For the other gas N_2, the extremely low absorption capacities at atmospheric pressure in both [Bmim][OAc] and the studied cosolvents imply that there are only

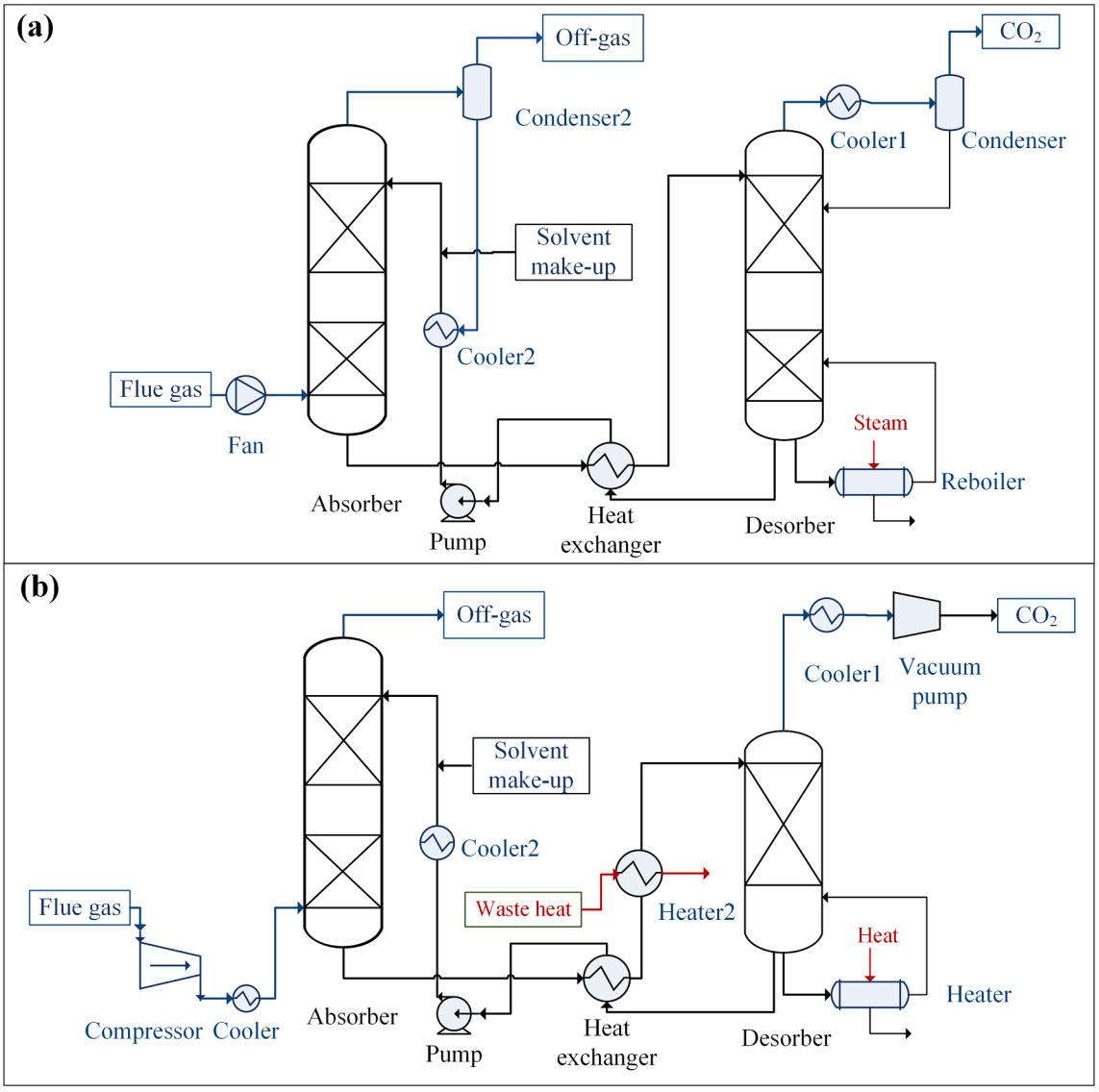

Fig. 2. Process flowsheet for CO_2 capture from flue gas based on chemical absorption. (a) Amine-based process; (b) IL-based process integrated with waste heat.

physical interactions. The schematic of gas–liquid equilibria with chemical interaction is depicted in Fig. 1.

For the contribution of physical absorption, it follows Henry's law, and the phase equilibria can be expressed as in Eq. (1).

$$Py_i\varphi_i^v = H_{i,s}(T,P)x_i\gamma_i/\gamma_i^{\infty} \tag{1}$$

where P is the system pressure, y_i is the mole fraction of gas i in the vapor phase, x_i is the mole fraction of gas i in the liquid phase, φ_i^v is the fugacity coefficient of gas i in the vapor phase, $H_{i,s}(T, P)$ is the Henry's constant of gas i in the solvent s at T and P, the subscript s is a pure solvent or mixed solvent, and γ_i^{∞} is the activity coefficient of gas i at infinite dilution in the liquid phase.

For the contribution of chemical absorption (i.e., chemical interaction between CO_2 and [Bmim][OAc]), the mechanism that two moles of [Bmim][OAc] chemically reacts with one mole of CO_2 to generate Bmim-2-carboxylate ([Bmim-2-COO]) [5] was adopted in this work, as shown in Fig. 1.

The chemical reaction equilibrium between CO_2 and [Bmim][OAc] is described in Fig. 1, and the chemical equilibrium constant K_{eq} of this reaction is expressed in Eq. (2).

$$K_{eq} = \frac{a_{[Bmim-2-COO]}}{a_{CO_2}\cdot\left(a_{[Bmim][OAc]}\right)^2} = \frac{x_{[Bmim-2-COO]}}{x_{CO_2}\cdot\left(x_{[Bmim][OAc]}\right)^2}\cdot\frac{\gamma_{[Bmim-2-COO]}}{\gamma_{CO_2}\cdot\left(\gamma_{[Bmim][OAc]}\right)^2} = exp\left(k_1+\frac{k_2}{T}\right) \tag{2}$$

where a is the activity in the liquid phase; K_{eq} is the chemical equilibrium constant.

As we can see from Fig. 1, due to the negligible vapor pressure of IL, it only exists in the liquid phase. In addition, the product (COOILn in Fig. 1) is only in the liquid phase. While the cosolvent follows Raoult's law in Eq. (3) and exists in both vapor and liquid phases:

$$Py_j\varphi_j^v = x_j\gamma_j P_j^s \tag{3}$$

where P_j^s is the vapor pressure of the cosolvent j.

The Henry's constant for gas i in the pure solvent j was calculated by the following equations:

$$H_{ij}(T,P) = H_{ij}(T)exp\left(\frac{PV_i^{\infty}}{RT}\right)$$
$$lnH_{ij}(T) = A_{ij} + B_{ij}/T \tag{4}$$

where H_{ij} (T) is the Henry's constant of gas i in the pure solvent j at the system temperature and pressure; V_i^{∞} is the infinite dilution partial volume of gas i.

The Henry's constant of gas i in the mixed solvent ($H_{i,\ mix}$) was calculated from those in the pure solvents as shown in Eq. (5) [17].

$$ln\left(\frac{H_{i,mix}}{\gamma_{i,mix}^{\infty}}\right)=\sum_j w_j ln\left(\frac{H_{ij}(T,P)}{\gamma_{ij}^{\infty}}\right)$$
$$w_j=\frac{x_j\left(V_{cj}\right)^{2/3}}{\sum_k x_k\left(V_{ck}\right)^{2/3}} \tag{5}$$

where w_j is the weighting factor; V_{cj} is the critical volume of the solvent j; $\gamma_{i,mix}^{\infty}$ and γ_{ij}^{∞} are the infinite dilution activity coefficients of gas i in the mixed solvent and pure solvent j, respectively.

The fugacity coefficient $\varphi_i{}^v$ of gas i in pure gas or a gas mixture was calculated by the Redlich-Kwong (RK) equation of state as shown in Eq. (6) with the parameters taken from Aspen databank.

$$ln\varphi_i^v=Z-1-ln(Z-BP)-(A^2/B)ln(1+BP/Z)$$
$$\begin{cases} P=\dfrac{RT}{V_m-b}-\dfrac{a}{T^{0.5}V_m(V_m+b)} \\ Z=PV_m/RT \\ A^2=a/R^2T^{2.5} \\ B=b/RT \\ a=\sum_i\sum_j y_iy_j(a_ia_j)^{0.5}, a_i=0.4278RT_{Ci}^{2.5}/P_{Ci} \\ b=\sum_i y_ib_i, b_i=0.08664RT_{Ci}/P_{Ci} \end{cases} \tag{6}$$

where R is the gas constant, V_m is the molar volume; a_i and a are the constants of a pure gas i and gas mixture, respectively, which correct for the attractive potential of molecules; b and b_i are the constants of a gas mixture and pure gas i, respectively, which correct for volume; and T_{Ci} and P_{Ci} are the critical temperatures and pressures for gas i, respectively.

The Non-Random Two-Liquid (NRTL) model was used to calculate the activity coefficient γ in the liquid phase by the following equation:

$$ln\gamma_i=\frac{\sum_{j=1}^m \tau_{ji}G_{ji}x_j}{\sum_{l=1}^m G_{li}x_l}+\sum_{j=1}^m\frac{G_{ij}x_j}{\sum_{l=1}^m G_{lj}x_l}\left[\tau_{ij}-\frac{\sum_{r=1}^m x_r\tau_{rj}G_{rj}}{\sum_{l=1}^m G_{lj}x_l}\right]$$
$$G_{ij}=exp\left(-c_{ij}\tau_{ij}\right),\ G_{ji}=exp\left(-c_{ji}\tau_{ji}\right) \tag{7}$$
$$\tau_{ij}=a_{ij}+b_{ij}/T,\ \tau_{ji}=a_{ji}+b_{ji}/T,\ c_{ij}=c_{ji}(i\neq j)$$

where m is the number of components, τ_{ij} is the NRTL binary interaction energy parameter, and c_{ij} is the non-randomness factor, which was fixed to be 0.2 in this work.

2.3. Process simulation and evaluation

2.3.1. Process description

The aqueous amine-based process was used as the benchmark, and its process flowsheet is depicted in Fig. 2a. It includes three main units, i.e., (1) Absorber, (2) Heat exchanger, and (3) Desorber.

(1) Absorber. In this part, CO_2 is chemisorbed by the liquid absorbent. The flue gas is fed to the bottom of the absorption column (block Absorber) by a flue gas fan, while the solvent is sprayed from the top of the absorber. The gas leaving from the top of the absorber was cooled to recycle the evaporated absorbent. The gas discharged from the top (stream Off-gas) of the absorber is mostly N_2.

(2) Heat exchanger. The CO_2-enriched solvent is passed through a heat exchanger to be preheated by the CO_2-lean solvent from the desorption unit before it flows to the top of the desorbed.

(3) Desorber. In this vessel, the CO_2-enriched solvent is regenerated by heating it up to a certain temperature (>383.15 K). The CO_2-lean solvent is then entered into a heat exchanger to preheat the CO_2-enriched solvent before being recirculated to the absorber. An extra cooler (block Cooler2) is usually needed to further decrease the temperature of the CO_2-lean solvent. The gas stream leaving from the top of the desorbed is passed through a cooler (block Cooler1) and a condenser to get high CO_2 concentrated gas.

Based on the amine-based process, the IL-based CO_2 capture process was adjusted, as shown in Fig. 2b. The gas compressor and cooler are added to increase the pressure of flue gas before fed into the absorber. In the desorption unit, a waste heat stream is used to preheat the CO_2-enriched solvent to 343.15 K with a heat exchanger (Heater2 in Fig. 2b). In addition, owing to the low vapor pressure of these IL hybrid solvents, the vacuum pump is added to reduce the pressure to less than 0.01 MPa to enhance desorption. The heater integrated with desorber is used to further provide the heat for reaching the required CO_2 lean loading.

2.3.2. Process simulation

The software Aspen Plus V11 (AspenTech, USA) was used to conduct process simulations. For the aqueous MEA-based system, the electrolyte non-random-two-liquid (eNRTL) model in Aspen Plus was used to model the physical properties, phase equilibria, and chemical reactions. The required parameters of the eNRTL model were adopted from the KEMEA data package, which is available in the Aspen Plus databank (V11) [19].

For the IL-based hybrid solvent systems, the NRTL-RK model was chosen as the thermodynamic model in Aspen Plus. The binary interaction parameters for calculating Henry's constants, reaction equilibrium constants, and activity coefficients were obtained by fitting the experimental data based on the theories described in Section 2.2. The methods of model parameterizing for the gas absorption capacity and other properties such as density and viscosity were provided in Section 3.2.1 and Section 3.2.3, respectively, together with the values of these model parameters. After that, these parameters were embedded in the Aspen Plus to carry out process simulation. The RADFRAC model in Aspen Plus (V11) was used to model the absorber and desorber. The Reactive-Distillation equilibrium reaction was used to define the chemical reaction between IL and CO_2 in the RADFRAC model.

The rate-based approach was used in the process simulation. The flue gas (1 kmol•s^{-1}) was composed of CO_2 (15 vol%) and N_2 (85 vol%), and it enters the absorber at 313.15 K, 0.1 MPa. The absorption using [Bmim][OAc]-DEPG250 was carried out at 308.15 K and 0.2 MPa in an absorber with a packing height of 30 m. While for the MEA process, the absorption was carried at 313.15 K and 0.1 MPa in absorber with 20 m packing height. The packing height in the desorption column was set to be 10 m for all the investigated absorbents. The metal pall ring with a diameter of 90 mm was selected as the packing material. The diameters of the absorber and desorber were calculated by keeping a fractional capacity of 80% in all cases.

2.3.3. Energy and cost estimation

For the chemical absorption process in Fig. 2a, the energy is utilized in three parts, that is, (1) the heating duty for solvent regeneration (Block Reboiler), (2) the electrical power required for the solvent pumps (Block Pump) and the flue gas fan (Block Fan), and (3) the cooling duty of the condensers in absorption (Block Condenser2) and solvent regeneration part (Block Condenser) and the coolers (Block Cooler1 and Cooler2). While for the process in Fig. 2b, the energy includes the electrical power for operating the solvent pump (Block Pump),

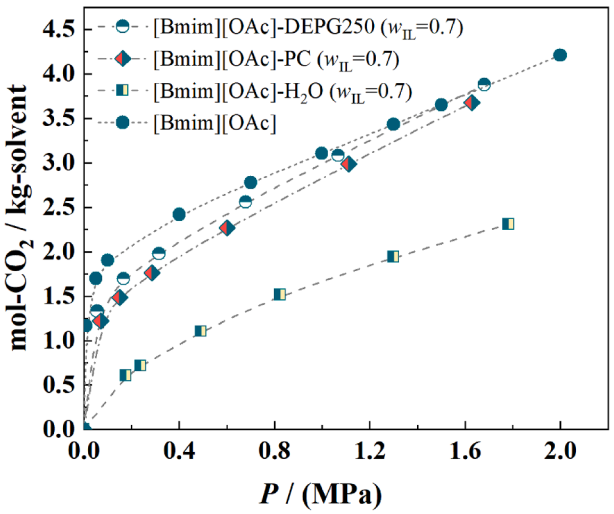

Fig. 3. CO_2 absorption capacities of [Bmim][OAc]-cosolvent systems with same mass fraction of IL (w_{IL}). Lines: a guide for eyes.

compressor (Block Compressor), and vacuum pump (Block Vacuum pump), as well as the heating duty for solvent regeneration (Block Heater) and the cooling duty of the coolers (Block Cooler, Cooler 1, and Cooler2). It should be mentioned that the amount of waste heat used to preheat the solvent is not included in accounting for the total energy usage.

Heating duty is often used as a comparison index in CO_2 capture from flue gas. Therefore, in this work, the electrical power was converted to heating duty, and the conversion efficiency of heat to electricity was set to be 0.3. The cooling duty and heating duty were calculated separately. The cost of the heating duty was determined by the cost of the steam, while the cost of cooling duty was calculated by the cost of the cooling water.

The total annual cost (TAC) is a summation of the annual capital cost (ACC) and the operation and maintenance cost (O&MC). The annual capital cost (ACC) was converted from the total capital cost (TCC), according to Eq. (8):

$$ACC = TCC \cdot \frac{ir(1+ir)^n}{(1+ir)^n - 1} \tag{8}$$

where the economic life n of the equipment is 15 years, and the interest rate ir is 9%.

The total capital cost (TCC) can be calculated using the method based on the percentage of equipment cost (EC), as summarized in our previous work [20]. Aspen Process Economic Analyzer (APEA) was used to determine the equipment cost by carrying out mapping, sizing, and evaluating. The operation and maintenance cost (O&MC) consists of the maintenance cost, operating supplies cost, research and development (R&D) cost, utility costs (i.e., electricity, steam, and cooling water), and absorbent replacement cost. In addition, in the O&MC estimation, an annual operation of 8600 h was used when calculating the operation cost. The hourly wage of the operators (hourly personnel cost) was set to be 42 \$•h^{-1} [20], corresponding to the results of the actual plant. The number of operators was calculated based on the equipment units, and five shifts for each operator were used. The price of electricity was set to be 0.10 \$•kWh^{-1}. The price of [Bmim][OAc] was estimated to be 20 \$•kg^{-1} [7]. The cost of MEA was set as 2.25\$•kg^{-1} [7]. The price of DEPG250 was set to be 3.5 \$•kg^{-1} [21]. The prices of cooling water and steam are 0.35 \$•GJ^{-1} and 20.5 \$•ton^{-1} [22,23], respectively. The cost of waste heat was set to be \$0.05 per GJ.

3. Results and discussions

3.1. Experimental results

The reliability of the experimental set-up was validated by comparing CO_2 absorption in water, propylene carbonate, [Bmim][OAc] and 1-Ethyl-3-methylimidazolium acetate ([Emim][OAc]) measured in this work and the data reported in the literature. The small deviation between the experimental data determined in this work and that reported in the literature proves the reliability of the measurement in this work. The detailed information is provided in supporting information (Fig. S1).

3.1.1. Cosolvent effect on the CO_2 absorption capacity

In this section, the CO_2 absorption capacity of [Bmim][OAc]-cosolvent was studied, where H_2O, propylene carbonate (PC), or DEPG250 was chosen as the cosolvent. The CO_2 absorption capacity of IL-cosolvent with the same [Bmim][OAc] content (mass fraction of IL $w_{IL} = 0.7$) at 298.15 K at different pressures (up to 1.9 MPa) was conducted. The experimental results are illustrated in Table S1 and Fig. 3.

For comparison, the CO_2 absorption capacity of pure [Bmim][OAc] at 298.15 K reported by Shiflett et al. [6] is also depicted in Fig. 3. As we can see from Fig. 3, the CO_2 absorption capacities of [Bmim][OAc]-cosolvent are lower than that of pure [Bmim][OAc], especially when the pressure is lower than 1 MPa. The CO_2 absorption capacities of [Bmim][OAc]-cosolvent follow the order: [Bmim][OAc]-DEPG250 > [Bmim][OAc]-PC > [Bmim][OAc]–H_2O. Water is a cheap and green

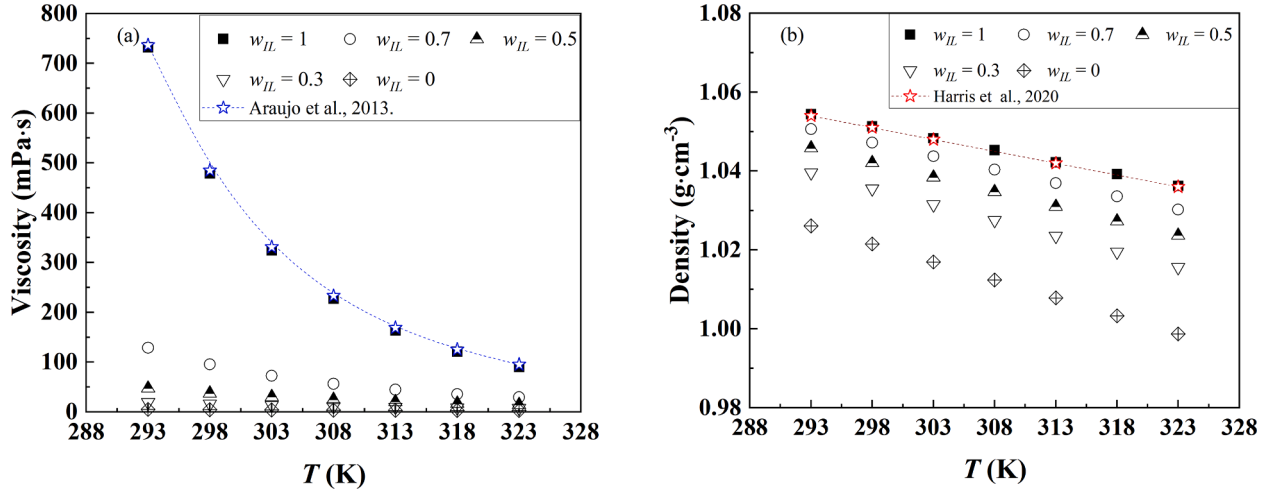

Fig. 4. The (a) viscosity and (b) density at different temperatures and mass fraction of IL (b) for [Bmim][OAc]-DEPG.

Table 1
CO_2 absorption capacity of [Bmim][OAc]-DEPG250 with different IL mass fractions at different temperatures.

P/ MPa	x_{CO2}	m_{CO2} /mol-CO_2/kg-solvent	P/ MPa	x_{CO2}	m_{CO2} /mol-CO_2/kg-solvent
w_{IL} = 0.3 at 298.15 K			w_{IL} = 0.5 at 298.15 K		
0.074	0.122	0.600	0.062	0.181	1.001
0.135	0.147	0.744	0.152	0.217	1.256
0.236	0.179	0.942	0.38	0.268	1.653
0.610	0.268	1.577	0.744	0.328	2.203
1.241	0.373	2.566	1.174	0.384	2.815
1.714	0.436	3.336	1.727	0.442	3.583
w_{IL} = 0.7 at 298.15 K			w_{IL} = 0.7 at 313.15 K		
0.057	0.219	1.325	0.072	0.192	1.127
0.171	0.261	1.668	0.164	0.227	1.391
0.314	0.292	1.953	0.421	0.277	1.810
0.609	0.336	2.398	0.733	0.320	2.224
1.056	0.389	3.006	1.283	0.374	2.823
1.631	0.444	3.779	1.824	0.420	3.423
w_{IL} = 0.7 at 328.15 K			w_{IL} = 0.7 at 328.15 K		
0.051	0.159	0.894	0.806	0.311	2.140
0.116	0.203	1.205	1.24	0.349	2.541
0.397	0.264	1.697	1.755	0.390	3.019

cosolvent, however, the addition of water leads to a significant decrease in CO_2 absorption capacity per kg-solvent. The hybrid solvent [Bmim][OAc]-DEPG250 shows the highest CO_2 absorption capacity amongst the studied hybrid solvents, and when the pressure is higher than 1 MPa, its CO_2 absorption capacity increases to the same as that of pure [Bmim][OAc]. The main reason is the high CO_2 absorption capacity of DEPG250 at high pressures. Therefore, [Bmim][OAc]-DEPG250 was selected for further investigation to study the effects of mass ratio and temperature at pressure from 0 to 1.9 MPa.

3.1.2. *Effects of mass ratio and temperature on density and viscosity*

Besides CO_2 absorption capacity, viscosity is another important factor that greatly affects mass transfer rate in absorption and desorption towers. Therefore, in this section, the viscosity of [Bmim][OAc]-DEPG250 with a different mass fraction of [Bmim][OAc] (w_{IL} from 0.3 to 0.7) was measured from 293.15 to 323.15 K. The data of pure [Bmim][OAc] were compared with that from the literature [24,25], showing the good consistency. The results are summarized in Table S2 (supporting information) and shown in Fig. 4a.

The monotonic decrease in viscosity was observed with the increase in temperature. According to Fig. 4a, at 308.15 K, when adding DEPG250 to [Bmim][OAc], forming a [Bmim][OAc]-DEPG250 mixture with the IL mass fraction (w_{IL}) of 0.7, the viscosity drastically drops from 227.1 to 56.4 mPa·s. Further decrease of the temperature to 298.15 leads to an increase in viscosity of [Bmim][OAc]-DEPG250 (w_{IL} = 0.7) to more than 100 mPa·s. The increase of DEPG250 mass fraction from 0.5 to 0.7 results in a further decrease of viscosities to 24.5 and 11.4 mPa·s, respectively. The densities of [Bmim][OAc]-DEPG250 with a different mass fraction of [Bmim][OAc] were also measured, and the results are shown in Fig. 4b. The densities of [Bmim][OAc]-DEPG250 at a certain mass ratio decrease linearly with the increase of temperature. The addition of DEPG250 leads to a slight reduction in density, and the density continuously decreases with the increase of the DEPG content.

3.1.3. *Effects of mass ratio, temperature, and pressure on the CO_2 absorption capacity*

To study how the content of DEPG250 affects the CO_2 absorption capacity in [Bmim][OAc]-DEPG250, the hybrid solvents with [Bmim][OAc] mass fractions of 0.3, 0.5, and 0.7 were selected. The effect of temperature on CO_2 absorption capacity was studied by conducting the experiment at three different temperatures (298.15, 313.15 and 328.15 K). The CO_2 absorption capacity at different temperatures and with different mass fractions of [Bmim][OAc] at the pressure up to 1.9 MPa is listed in Table 1 and shown in Fig. 5. In addition, the CO_2 absorption capacity of pure [Bmim][OAc] at 298.15 K [6] and the newly measured CO_2 absorption capacity of DEPG250 at 298.15 K are also shown in Fig. 5a.

Within the investigated pressure ranges from 0 to 1.9 MPa, the CO_2 absorption capacity increases with increasing [Bmim][OAc] content. With the increase of pressure, the difference among the solvents with different mass fractions decreases gradually. For these hybrid solvents, the CO_2 absorption capacity of [Bmim][OAc]-DEPG250 with w_{IL} = 0.7 at 0.1 MPa reaches 1.4 mol-CO_2/kg-solvent, which is 2.3 and 1.3 times those of the solvents with w_{IL} = 0.3 and w_{IL} = 0.5, respectively, that is, 0.62 and 1.0 mol-CO_2/kg-solvent, respectively. The CO_2 absorption capacity increases dramatically when the pressure is lower than 0.2 MPa due to the chemisorption of [Bmim][OAc]. After that, when the pressure is larger than 0.2 MPa, it increases linearly with increasing pressure, which behaves the characteristic of physical absorption. When the pressure is 1.9 MPa, the CO_2 absorption capacity of [Bmim][OAc]-DEPG250 with w_{IL} = 0.7 increases to 4.2 mol-CO_2/kg-solvent, and those of [Bmim][OAc]-DEPG250 with w_{IL} = 1, w_{IL} = 0.5, and w_{IL} = 0.3 are 4.2, 3.7, and 3.5 mol-CO_2/kg-solvent, respectively. Besides the mass ratio between [Bmim][OAc] and DEPG250, the gas absorption capacity of these hybrid solvents may also be influenced by the binary interactions between [Bmim][OAc] and DEPG250. Thermodynamic modeling was carried out and described in Section 3.2.1 to quantify

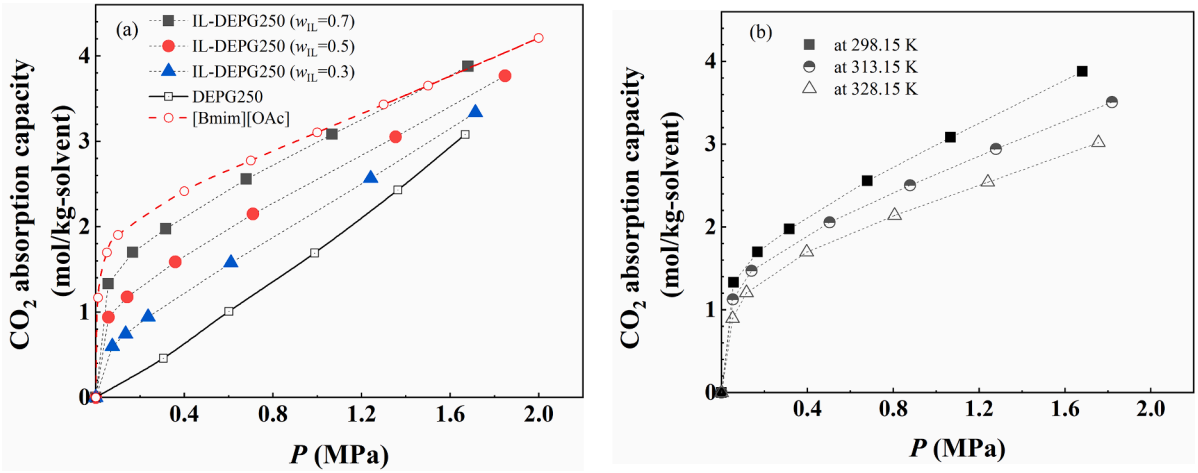

Fig. 5. CO_2 absorption capacity of [Bmim][OAc]-DEPG250 binary systems (a) with different w_{IL} at 298.15 K, and (b) with same w_{IL} but different temperatures. Lines: a guide for eyes.

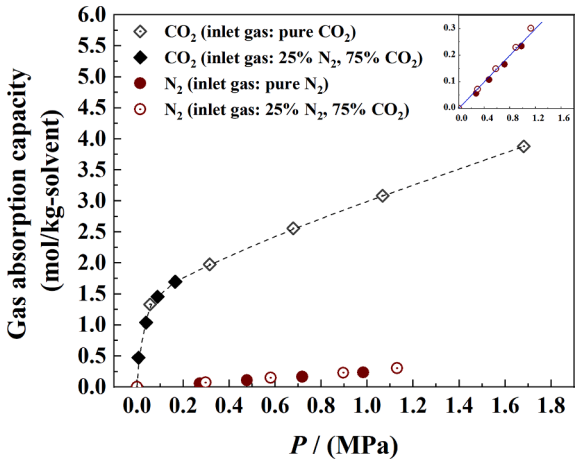

Fig. 6. Gas absorption capacity of [Bmim][OAc]-DEPG with w_{IL} of 0.7 at 298.15 K with different inlet gas streams.

different effects.

Temperature is also an essential factor in CO_2 absorption. Therefore, the effect of temperatures on the CO_2 absorption capacity was studied for the [Bmim][OAc]-DEPG250 with $w_{IL}$of 0.7. The results are summarized in Table 1 and shown in Fig. 5b. It is clear to observe that the CO_2 absorption capacity decreases with increasing temperature. When the temperature rises from 298.15 to 328.15 K, the CO_2 absorption capacity at 0.1 MPa slightly drops from 1.51 to 1.1 mol-CO_2/kg-solvent. With the increase of pressure, the difference between different temperatures increases greatly. For instance, the CO_2 absorption capacity decreases from 3.72 to 2.78 mol-CO_2/kg-solvent at 1.6 MPa when the temperature increases from 298.15 to 328.15 K. This means that a low temperature is favored in terms of CO_2 absorption capacity, and the absorption capacity is more sensitive to temperature at high pressures.

3.1.4. N_2 Absorption capacity and the effect of type of gas stream on the gas absorption capacity

Both pure [Bmim][OAc] and DEPG250 have been proved to have low solubility on N_2. This part is to investigate the N_2 absorption capacity in [Bmim][OAc]-DEPG250. The absorption capacities of pure N_2 in [Bmim][OAc]-DEPG250 with w_{IL} of 0.7 at 298.15 K were measured. Furthermore, the CO_2 and N_2 absorption capacities at 298.15 K with the flue gas (with 75 % N_2 and 25% CO_2) as an inlet gas were also measured. The experimental data are summarized in Table S3 and Table S4 (supporting information) and shown in Fig. 6.

As can be seen from Fig. 6, the N_2 solubilities increase linearly with increasing pressure, indicating physical absorption of N_2 in [Bmim][OAc]-DEPG250. Compared with the CO_2 absorption capacity, the N_2 absorption capacity in [Bmim][OAc]-DEPG250 stays at an extremely low level. The difference between N_2 and CO_2 absorption capacities changes with pressure. For example, at 0.1 MPa, the CO_2 absorption capacity is 1.50 mol-CO_2/kg-solvent, which is 60 times higher than that of N_2 (0.025 mol-N_2/kg-solvent). When the pressure increases to 0.8 MPa, the N_2 absorption capacity is about 0.2 mol-N_2/kg-solvent at 1 MPa, while the CO_2 absorption capacity is nearly 2.72 mol-CO_2/kg-solvent, which is 13.6 times higher than those of N_2. This result shows that low pressure favors the selectivity of CO_2 over N_2.

The CO_2 and N_2 absorption capacities for the gas mixture as the inlet gas are almost the same as those when the inlet gas is pure gas. This implies that the N_2 existing in the gas stream has a negligible effect on the CO_2 absorption capacities, likewise, the N_2 absorption capacities are not affected by the CO_2 existing in the gas stream.

3.2. Thermodynamic modeling results

3.2.1. Modeling gas absorption capacity

Based on the theory described in section 2.2 and the experimental data determined in section 3.1, thermodynamic modelling was carried out. To model the CO_2 solubility in [Bmim][OAc]-DEPG250, Henry's constant of CO_2, the chemical equilibrium constant K_{eq}, and activity coefficients are required. The Henry's constant of CO_2 in [Bmim][OAc]-DEPG250 was obtained from those in DEPG250 and [Bmim][OAc], where the critical volumes V_C of DEPG250 and [Bmim][OAc] are the only needed parameters as shown in Eq. (5). To estimate the critical volumes V_C, the group contribution method, that is, the modified Lydersen-Joback-Reid method [26] was used. Besides V_C, the other properties such as critical properties (T_C, P_C, Z_C), boiling point (T_b), molecular weight (M_W) as well as an acentric factor (w) for DEPG250 and [Bmim][OAc] are also necessary input to define a non-databank component in Aspen Plus. The estimated values are listed in Table 2. The groups that contributed to estimating these properties of DEPG250 and [Bmim][OAc] are listed in Table S8 (supporting information). The model equations for estimating these properties are provided in Eqs. (S1-S4) in supporting information.

Henry's constants of CO_2 in pure DEPG250 at different temperatures reported by Henni *et al.*[27] were used to obtain the parameters (A_{ij}, B_{ij}) in Eq. (4) by setting the binary interaction parameters (a_{ij}, b_{ij}) in Eq. (7) between CO_2 and DEPG250 to be 0. The newly measured CO_2 solubility data of pure DEPG250 (Table S5) were used to verify these parameters, showing good agreement with the predicted data (*ARD* less than 8%). For [Bmim][OAc], the parameters (k_1, k_2) for calculating K_{eq} were directly taken from the literature [6]. Meanwhile, the parameters (A_{ij}, B_{ij}) for calculating Henry's constant of CO_2 in [Bmim][OAc] were obtained by the regression of the CO_2 solubility data in pure [Bmim][OAc] reported by Shiflett et al.[6] After that, the parameters (a_{ij}, b_{ij}) for determining the NRTL binary parameters (τ_{ij}) in Eq. (7) were set as adjustable parameters by regression of the experimental data of gas absorption capacities in [Bmim][OAc]-DEPG250 mixtures with different mass ratios at different temperatures. During the fitting of (a_{ij}, b_{ij}), the previously obtained parameters (A_{ij}, B_{ij}) in Eq. (4) for calculating Henry's constants of CO_2 in pure cosolvent and [Bmim][OAc], the parameters (k_1, k_2) for calculating K_{eq}, and V_C of pure cosolvent and [Bmim][OAc] were set as the fixed values.

To model N_2 absorption capacity in [Bmim][OAc]-DEPG250 system, the corresponding Henry's constant of N_2 and activity coefficients are required. The parameters (A_{ij}, B_{ij}) for calculating $H_{i,j}$ (T) of N_2 in DEPG250 were taken from our previous work [18]. After that, the obtained parameters (A_{ij}, B_{ij}) were set as fixed values, and NRTL binary parameters between N_2 and DEPG250 (τ_{ij}) in Eq. (7) were set to be the adjustable parameters to fit the solubility data at relatively high pressures (i.e., above 1 MPa).

Afterwards, the above-obtained parameters (A_{ij}, B_{ij}) for calculating $H_{i,j}$ (T) of N_2 in DEPG250, (a_{ij}, b_{ij}) for obtaining the NRTL binary interactions between N_2 and DEPG250, and (a_{ij}, b_{ij}) for calculating the NRTL binary interactions between [Bmim][OAc] and DEPG250 were set to be fixed values, and the parameters (A_{ij}, B_{ij}) for calculating Henry's constants of N_2 in [Bmim][OAc] were set as adjustable parameters and obtained from the fitting of the experimental results of the pure N_2

Table 2
The estimated properties for DEPG250 and [Bmim][OAc].

Properties	*Mw*/g/mol	T_C/K	T_b/K	P_C/MPa	V_C/m^3/kmol	Z_C	*w*
DEPG250	250.00	777.153	583.400	1.929	0.757	0.226	0.661
[Bmim][OAc]	198.3	847.3	624.6	2.45	0.658	0.2285	0.668

Table 3
The model parameters for modeling the gas absorption capacity of DEPG250 and/or [Bmim][OAc]

Solute i	Solvent j	$\ln H_{ij}$ /MPa		$\ln K_{eq}$		τ_{ij}	
		A_{ij}	B_{ji}	k_1	k_2	a_{ij}	b_{ji}
CO_2	DEPG250	8.06	−2060.20	—	—	0	0
DEPG250	CO_2	—	—	—	—	0	0
N_2	DEPG250	9.92	−2006.70	—	—	0.81	−305.54
DEPG250	N_2	—	—			1.06	−207.91
CO_2	[Bmim][OAc]	6.33	−1437.37	−9.72	4509.26	0.00	0.00
CO_2	[Bmim-2-COO]	6.33	−1437.37	—	—	0.00	0.00
N_2	[Bmim][OAc]	11.34	−2486.67	—	—	0.00	0.00
N_2	[Bmim-2-COO]	11.34	−2486.67	—	—	0.00	0.00
DEPG250	[Bmim][OAc]	—	—	—	—	31.39	−10363.50
[Bmim][OAc]	DEPG250	—	—	—	—	−37.71	12118.3

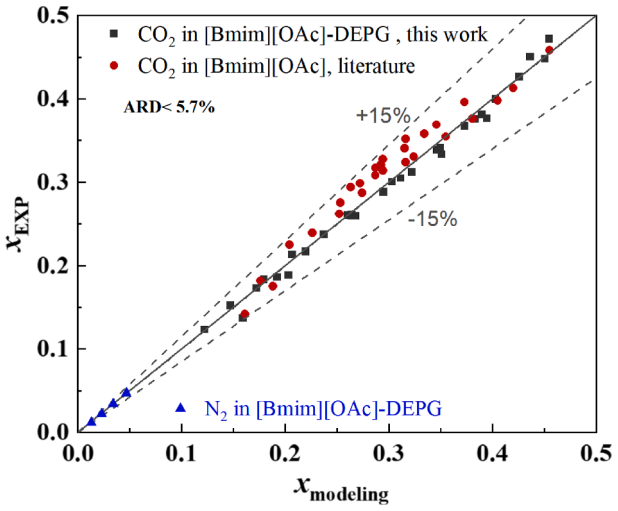

Fig. 7. Parity plot for [Bmim][OAc]-DEPG250-CO_2 /N_2 system, x_i: experiment vs. modeling.

absorption capacities at 298.15 K in [Bmim][OAc]-DEPG250.

All the obtained parameters are listed in Table 3. Obviously, according to the results illustrated in Fig. 7, the modeling results are in good agreement with the experimental data with average relative deviations (*ARD*) of 5.7% and 3.0% for CO_2 and N_2, respectively. It means that the thermodynamic modeling results of CO_2 or N_2 solubility in [Bmim][OAc]- DEPG250 mixtures are reliable.

3.2.2. *Further analysis*

The CO_2 solubility and the concentration of different species in the system were predicted by thermodynamic modeling with the obtained parameters (Table 3). The physical and chemical contributions to CO_2 solubility of the [Bmim][OAc]-DEPG250 systems with different mass ratios and at different temperatures were analyzed. The results are illustrated in Fig. 8.

For pure [Bmim][OAc], the chemical contribution is dominated (greater than80%) when the pressure is less than 1 MPa. With the increase of pressure, the physical contribution increases. Adding DEPG250 increases the physical contribution significantly. The increase of the DEPG250 mass ratio and the decrease of temperature favor the contribution of physisorption, while it shows the opposite effects on the contribution of chemisorption. When the pressure is lower than 0.4 MPa, chemisorption contributes 70% of the total CO_2 absorption capacity for the solvent [Bmim][OAc]-DEPG250 (w_{IL} = 0.3), which is 25% lower than that for pure [Bmim][OAc]. These results imply that under the same condition, the regeneration process of the solvent with a higher mass fraction of DEPG250 requires less energy because of the decreased chemisorption contribution. On the other hand, the increase in temperature leads to a negligible change in both physical and chemical contributions when the pressure is less than 0.4 MPa. The negligible change means that the absorption and/or desorption is insensitive to the temperature at low pressures. With increasing pressure, the increase in temperature leads to a slight decrease and increase in physical and chemical contributions, respectively. The reason is that the absorption contributed from the physical absorption is more sensitive to the temperature than that from the chemical reaction, even though the increase of temperature results in a decreased CO_2 absorption capacity caused by both chemical and physical absorptions.

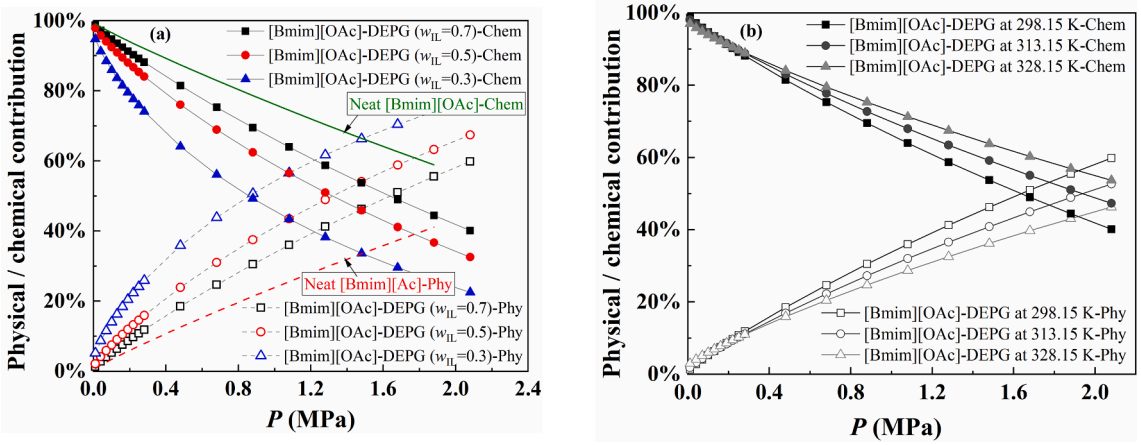

Fig. 8. The mass fraction of [Bmim][OAc] (a) and temperature (b) effects on the physical and chemical contributions to CO_2 absorption capacity changing with pressure.

Table 4
Equations for temperature-dependent properties.*

Property	Equations	No
Liquid molar volume V_m (M_w/ρ)	$V_m = C_1 + C_2T + C_3T^2$	(9–1)
Viscosity η	$\eta = C_1 + C_2T + C_3T^2$	(9–2)
Heat capacity C_p	$C_P = C_1 + C_2T + C_3T^2$	(9–3)
Surface tension σ	$\sigma = C_1(1 - T/T_C)^{C_2+C_3T/T_C}$	(9–4)
Vapor pressure P_L	$lnP_L = C_1 + C_2/T + C_3lnT$	(9–5)

* C_1, C_2, and C_3 are the parameters describing these properties in Aspen Plus; T is in Kelvin.

3.2.3. Other properties

The equations used to model the temperature-dependent properties are listed in Table 4. The densities of pure [Bmim][OAc] and DEPG250 at various temperatures newly measured in this work (Table S2) were converted to liquid molar volume first, and then the data of liquid molar volume were used to regress the adjustable parameters of Eq. (9–1) in Table 4. The newly measured viscosities of pure [Bmim][OAc] and DEPG250 at various temperatures (in Table S2) were used to regress the adjustable parameters of Eq. (9–2) in Table 4. The adjustable parameters of Eq. (9–3) describing the heat capacity of [Bmim][OAc] were regressed by the data reported from the literature. The surface tension of [Bmim][OAc] reported in the literature was used to obtain the adjustable parameters of Eq. (9–4). The heat capacity, surface tension, and vapor pressure of DEPG250 were assumed to be the same as that of DEPG280 estimated by Aspen Plus, and these data were used to get the adjustable parameters of Eq. (9–3), Eq. (9–4), and Eq. (9–5) for DEPG250. The obtained parameters are listed in Table S6. Additionally, the newly measured density and viscosity of hybrid solvents were used to get the binary parameters in modeling the excess properties of the mixed solvents (Table S7 in supporting information).

3.3. Process evaluation and comparison

Based on the same solvent regeneration degree (~50%), the performance of the process using [Bmim][OAc]-DEPG250 with a different mass content of [Bmim][OAc] (w_{IL} from 0.35 to 0.7) was obtained and compared with the process of aqueous MEA (30 wt% MEA). During the simulation, the mass flow rate of solvent was adjusted to meet the requirement of the 90% CO_2 removal rate. The desorption pressure of the desorber was adjusted to reach a 50% solvent regeneration degree. The results are shown in Fig. 9.

The required desorption pressure continuously increases when the mass fraction of IL changes from 0.7 to 0.35. The reason is that the increase of the DEPG250 mass content increases the contribution of physisorption, which needs less energy (higher vacuum pressure) to be regenerated to the same degree. The required total heating duty decreases first and then starts to increase when the mass fraction of IL changes from 0.7 to 0.35. The minimum value shows at the mass fraction of IL of 0.6. In addition, for aqueous MEA solution, at 50% solvent regeneration degree, CO_2 purity in the recovered gas is 90%. For [Bmim]

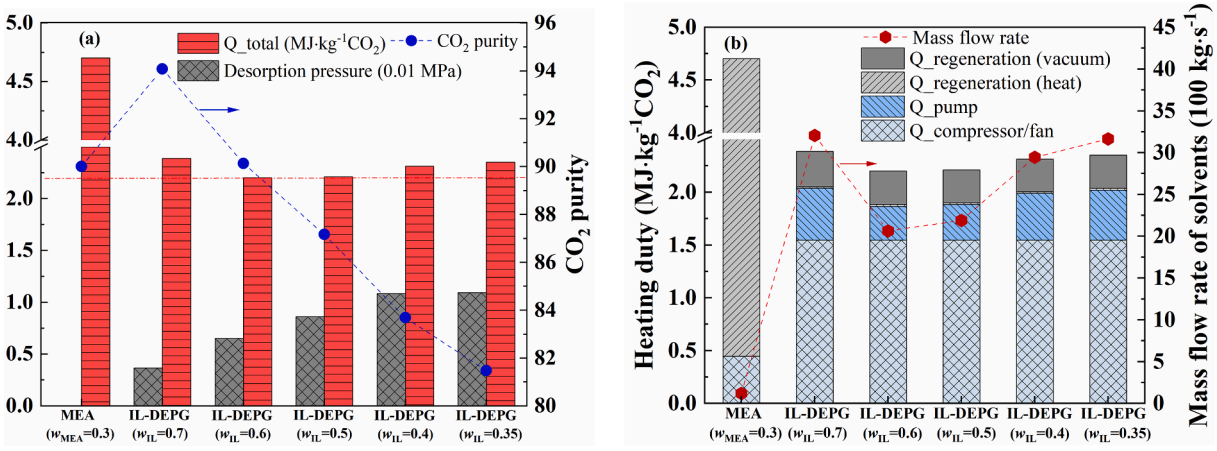

Fig. 9. (a) Total heating duty, desorption pressure, and CO_2 purity in the recovered gas, (b) heating duty from different units and mass flow rates of solvents, of the processes using IL-DEPG250 hybrid solvents and aqueous MEA solution as the absorbents.

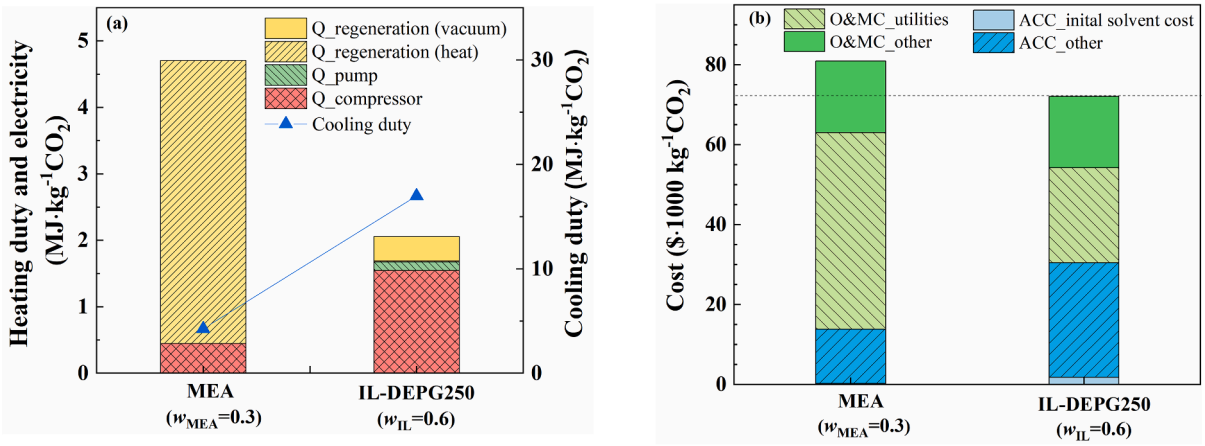

Fig. 10. (a) Heating duty and (b) cost of CO_2 capture from flue gas using different solvents when the CO_2 purity of the recovered gas is 94%.

[OAc]-DEPG250, the CO_2 purity in the recovered gas continuously decreases with increasing the DEPG250 mass fraction. The main reason is that with the increase of the DEPG250 content, the N_2 absorption capacity of the hybrid solvent increases. Therefore, under the same regeneration degree of the solvent, more N_2 is desorbed, leading to a decreased CO_2 purity. When the mass fraction of IL is less than 0.6 or the DEPG250 mass fraction is larger than 0.4, the CO_2 purity is less than 90% at this solvent regeneration degree.

Meanwhile, as we can see from Fig. 9b, the required mass flow rate of the solvent decreases dramatically to a minimum value with the increase of DEPG250 content. After that, it starts to increase gradually. The extreme value shows at the mass fraction of IL is 0.6, which is around 20 times that of the aqueous MEA solution. The showing of extreme value is due to the dual effect of the decreased CO_2 absorption capacity and the decreased viscosity with the addition of DEPG250. The results of heating duty show that the hybrid solvents ([Bmim][OAc]-DEPG250) only utilize less than 50% of the heating duty of aqueous MEA solution because of the low-pressure desorption and preheating with waste heat in this hybrid solvent-based process. The lowest heating duty is for the hybrid solvents with an IL mass fraction of 0.6. Either increase or decrease of IL mass fraction increases the heating duty due to the increased work from the solvent pump caused by the increased solvent amount.

Therefore, [Bmim][OAc]-DEPG250 with IL mass fractions of 0.6 were selected for further study at higher CO_2 purity in the recovered gas. It should be mentioned that CO_2 purity in the recovered gas was adjusted by increasing solvent regeneration degree. However, the existence of the desorbed N_2 makes it can not reach 95% CO_2 purity. Therefore, 94% CO_2 purity was used in this work. To reach this purity, the CO_2 regeneration degree of the solvent was about 89.7%. In addition, during the simulation the capture ratio of CO_2 from the inlet gas stream (CO_2 removal rate) was kept at 90% by adjusting the mass flow rate of the solvent. The results are compared with those of the aqueous MEA solution. As we can see from Fig. 10a, adding DEPG250 as a cosolvent greatly decreases the total heating duty by 56% compared with that of the aqueous MEA process. However, the cooling duty is greatly increased due to the large amount of circulated solvent used in the process. As a consequence, the utility costs of [Bmim][OAc]-DEPG250 with the IL mass fractions of 0.6 decrease by 52% compared with that of aqueous MEA solution (Fig. 10b). On the other hand, the annual capital cost (ACC) of [Bmim][OAc]-DEPG250 is higher than that of the aqueous MEA solution. One of the reasons is the high cost of gas compressors used in the absorption process. It is needed to compress the gas entering the absorber because a slightly high pressure was used in the absorber in order to increase the gas absorption capacity in the absorption unit. Another reason is the high cost of the heat exchangers caused by the large heat exchanging areas needed in the process using [Bmim][OAc]-DEPG250. Specifically, the mass flow rate of the solvent in the process using [Bmim][OAc]-DEPG250 (i.e., 848.11 kgs^{-1}) is about seven times that using aqueous MEA solution (i.e., 119.72 kgs^{-1}). Therefore, the heat exchanger with a larger heat exchanging area in the process using [Bmim][OAc]-DEPG250 is needed compared to that using the aqueous MEA solution when the heat transfer coefficient and temperature gradient are similar. The initial solvent cost only slightly affects ACC. Using hybrid solvents finally leads to a decreased total capture cost per 1000 kg CO_2 captured. The capture cost of [Bmim][OAc]-DEPG250 with the IL mass fractions of 0.6 reduces 11% compared to that of aqueous MEA solution. The main advantage of using these hybrid solvents is that low regeneration temperature is required, which allows using low-grade waste heat to preheat and thus reduces the heating duty from steam.

4. Conclusions

In this work, the CO_2 absorption capacity of [Bmim][OAC] formulated hybrid solvents with water, DEPG, or PC as a cosolvent was studied and compared. The one with DEPG250 shows the highest value, indicating DGPG is a preferable cosolvent for [Bmim][OAC]. The increases in the mass content of DEPG250 and temperature decrease the CO_2 absorption capacity, meanwhile decrease the viscosity, indicating an increase in mass transfer rate. The comparison of the N_2 and CO_2 absorption capacities in [Bmim][OAc]-DEPG250 with the simulated flue gas as the feed gas and that using pure gas as a feed gas shows that the type of gas stream, that is, pure gas or gas mixture, has a negligible effect on the N_2 and CO_2 absorption capacity. Thermodynamic modeling based on the NRTL-RK model and chemical reaction equilibrium between CO_2 and [Bmim][OAc] shows a good agreement with experimental data. The process integrated with waste heat was designed for this hybrid solvent, and the hybrid solvent with a mass fraction of IL 0.6 achieves the lowest heating duty. Further decrease or increase of IL mass fraction increases not only the solvent amount but also the energy usage because of the increased work from the solvent pump and vacuum compressor. The techno-economic analysis shows that when the CO_2 removal rate is 90%, and the CO_2 purity of recovered gas is 94%, the process using [Bmim][OAc]-DEPG250 with IL mass fraction of 0.6 decreases 52% of utility cost and reduces 11% of capture cost compared with the aqueous amine-based process. The results also show that the high equipment cost from the gas compressor and heat exchangers is the main reason diminishing the advantage of this hybrid solvent. Future works will be focused on process optimization and sensitivity analysis.

CRediT authorship contribution statement

Chunyan Ma: Conceptualization, Investigation, Methodology, Writing – original draft, Writing – review & editing. **Nan Wang:** Investigation, Writing – original draft, Writing – review & editing. **Nannan Ye:** Investigation. **Xiaoyan Ji:** Conceptualization, Writing – original draft, Writing – review & editing.

Declaration of Competing Interest

The authors declare that they have no known competing financial interests or personal relationships that could have appeared to influence the work reported in this paper.

Acknowledgement

This work was supported by the Swedish Energy Agency (Energimyndigheten) (P50830-1).

Appendix A. Supplementary material

Supplementary data to this article can be found online at https://doi.org/10.1016/j.apenergy.2021.117767.

References

[1] Rochelle GT. Amine scrubbing for CO2 capture. Science 2009;325(5948):1652–4.
[2] Brennecke JF, Gurkan BE. Ionic liquids for CO2 capture and emission reduction. J Phys Chem Lett. 2010;1(24):3459–64.
[3] Zhang X, Zhang X, Dong H, Zhao Z, Zhang S, Huang Y. Carbon capture with ionic liquids: overview and progress. Energy Environ Sci. 2012;5(5):6668. https://doi.org/10.1039/c2ee21152a.
[4] Maginn EJ. Design and evaluation of ionic liquids as novel CO2 absorbents. Quarterly Technical Report to DOE. 2005:1–12.
[5] Yokozeki A, Shiflett MB, Junk CP, Grieco LM, Foo T. Physical and chemical absorptions of carbon dioxide in room-temperature ionic liquids. J Phys Chem B. 2008;112(51):16654–63.
[6] Shiflett MB, Kasprzak DJ, Junk CP, Yokozeki A. Phase behavior of carbon dioxide plus [bmim][Ac] mixtures. J Chem Thermodyn 2008;40:25–31.
[7] Shiflett MB, Drew DW, Cantini RA, Yokozeki A. Carbon dioxide capture using ionic liquid 1-butyl-3-methylimidazolium acetate. Energ Fuel 2010;24(10):5781–9.
[8] Nguyen TBH, Zondervan E. Ionic liquid as a selective capture method of CO2 from different sources: comparison with MEA. ACS Sustain Chem Eng 2018;6(4):4845–53.
[9] Fendt S, Padmanabhan S, Blanch HW, Prausnitz JM. Viscosities of acetate or chloride-based ionic liquids and some of their mixtures with water or other common solvents. J Chem Eng Data 2011;56(1):31–4.

[10] Wang Y, Ma C, Liu C, Lu X, Feng X, Ji X. Thermodynamic study of choline chloride-based deep eutectic solvents with water and methanol. J Chem Eng Data 2020;65(5):2446–57.
[11] Seo S, Quiroz-Guzman M, DeSilva MA, Lee TB, Huang Y, Goodrich BF, et al. Chemically tunable ionic liquids with aprotic heterocyclic anion (AHA) for CO2 capture. J Phys Chem B 2014;118(21):5740–51.
[12] Ventura SPM, Pauly J, Daridon JL, da Silva JAL, Marrucho IM, Dias AMA, et al. High pressure solubility data of carbon dioxide in (tri-iso-butyl(methyl) phosphonium tosylate plus water) systems. J Chem Thermodyn 2008;40:1187–92.
[13] Wang G, Hou W, Xiao F, Geng J, Wu Y, Zhang Z. Low-viscosity triethylbutylammonium acetate as a task-specific ionic liquid for reversible CO2 absorption. J Chem Eng Data 2011;56(4):1125–33.
[14] Alonso G, Gamallo P, Sayós R, Llovell F. Combining soft-SAFT and COSMO-RS modeling tools to assess the CO2-SO2 separation using phosphonium-based ionic liquids. J Mol Liq 2020;297:111795. https://doi.org/10.1016/j.molliq.2019.111795.
[15] Li X, Hou M, Zhang Z, Han B, Yang G, Wang X, et al. Absorption of CO2 by ionic liquid/polyethylene glycol mixture and the thermodynamic parameters. Green Chem 2008;10(8):879. https://doi.org/10.1039/b801948g.
[16] Lepre LF, Pison L, Siqueira LJA, Ando RA, Costa Gomes MF. Improvement of carbon dioxide absorption by mixing poly(ethylene glycol) dimethyl ether with ammonium-based ionic liquids. Sep Purif Technol 2018;196:10–9.
[17] Ma C, Shukla SK, Samikannu R, Mikkola J-P, Ji X. CO2 separation by a series of aqueous morpholinium-based ionic liquids with acetate anions. ACS Sustain Chem Eng 2020;8(1):415–26.
[18] Wang N, Ma C, Yu H, Ji X. Thermodynamics of CO2 separation with the superbase derived ionic liquid Organic solvent binary system. J Mol Liq 2021;331:115760. https://doi.org/10.1016/j.molliq.2021.115760.
[19] Huang Y, Zhang X, Zhang X, Dong H, Zhang S. Thermodynamic modeling and assessment of ionic liquid-based CO2 capture processes. Ind Eng Chem Res 2014;53(29):11805–17.
[20] Xie Y, Björkmalm J, Ma C, Willquist K, Yngvesson J, Wallberg O, et al. Techno-economic evaluation of biogas upgrading using ionic liquids in comparison with industrially used technology in Scandinavian anaerobic digestion plants. Appl Energy 2018;227:742–50.
[21] Ma C, Liu C, Lu X, Ji X. Techno-economic analysis and performance comparison of aqueous deep eutectic solvent and other physical absorbents for biogas upgrading. Appl Energy 2018;225:437–47.
[22] Aromada SA, Eldrup NH, Normann F, Øi LE. Techno-economic assessment of different heat exchangers for CO2 capture. Energies 2020;13(23):6315. https://doi.org/10.3390/en13236315.
[23] Ali H, Eldrup NH, Normann F, Skagestad R, Øi LE. Cost estimation of CO2 Absorption plants for CO2 mitigation – method and assumptions. Int J Greenh Gas Control. 2019;88:10–23.
[24] Araújo JMM, Pereiro AB, Alves F, Marrucho IM, Rebelo LPN. Nucleic acid bases in 1-alkyl-3-methylimidazolium acetate ionic liquids: a thermophysical and ionic conductivity analysis. J Chem Thermodyn 2013;57:1–8.
[25] Harris KR. Temperature and pressure dependence of the viscosity of the ionic liquid 1-butyl-3-methylimidazolium acetate. J Chem Eng Data. 2020;65(2):804–13.
[26] Valderrama JO, Robles PA. Critical properties, normal boiling temperatures, and acentric factors of fifty ionic liquids. Ind Eng Chem Res 2007;46(4):1338–44.
[27] Henni A, Tontiwachwuthikul P, Chakma AJTCJoCE. Solubilities of carbon dioxide in polyethylene glycol ethers. 2005;83:358-61.